Genomic landscape of pediatric adrenocortical tumors

HHS Public Access

Author manuscript

Nat Commun. Author manuscript; available in PMC 2015 September 06.

Published in final edited form as:

Nat Commun. ; 6: 6302. doi:10.1038/ncomms7302.

Genomic landscape of pediatric adrenocortical tumors

Emilia M. Pinto[1,*], **Xiang Chen**[2,*], **John Easton**[2], **David Finkelstein**[2], **Zhifa Liu**[3], **Stanley Pounds**[3], **Carlos Rodriguez-Galindo**[4], **Troy C. Lund**[5], **Elaine R. Mardis**[6,7,8], **Richard K. Wilson**[6,7,9], **Kristy Boggs**[2], **Donald Yergeau**[2], **Jinjun Cheng**[2], **Heather L. Mulder**[2], **Jayanthi Manne**[2], **Jesse Jenkins**[10], **Maria J. Mastellaro**[11], **Bonald C. Figueiredo**[12], **Michael A. Dyer**[13], **Alberto Pappo**[14], **Jinghui Zhang**[2,+], **James R. Downing**[10], **Raul C. Ribeiro**[14,*,+], and **Gerard P. Zambetti**[1,*,+]

[1]Department of Biochemistry, St. Jude Children's Research Hospital, Memphis, TN, USA

[2]Department of Computational Biology and Bioinformatics, St. Jude Children's Research Hospital, Memphis, TN, USA

[3]Department of Biostatistics, St. Jude Children's Research Hospital, Memphis, TN, USA

[4]Department of Pediatric Oncology, Dana-Farber/Boston Children's Cancer and Blood Disorders Center and Department of Pediatrics, Harvard Medical School, Boston, MA, USA

[5]University of Minnesota Medical School, Minneapolis, MN, USA

[6]The Genome Institute, Washington University School of Medicine, St Louis, MO, USA

[7]Department of Genetics, Washington University School of Medicine, St Louis, MO, USA

[8]Department of Medicine, Washington University School of Medicine, St Louis, MO, USA

[9]Department of Siteman Cancer Center, Washington University School of Medicine, St Louis, MO, USA

[10]Department of Pathology, St. Jude Children's Research Hospital, Memphis, TN, USA

[11]Boldrini Children's Research Hospital, Campinas, Brazil

[12]Instituto de Pesquisa Pelé Pequeno Príncipe, Curitiba, Brazil

[13]Department of Developmental Neurobiology, St. Jude Children's Research Hospital, Memphis, TN, USA

[+]Correspondence should be addressed to GPZ (gerard.zambetti@stjude.org); RCR (raul.ribeiro@stjude.org); or JZ (jinghui.zhang@stjude.org).

[*]These authors contributed equally to the work.

Author contributions

G.P.Z, R.C.R., J.Z., E.M.P., X.C., E.R.M., R.K.W., and J.R.D. designed experiments or supervised research. M.J.M. provided samples. R.C.R. carried out chart review for clinical information. E.M.P., J.E., K.B., D.Y., J.C., T.C.L., J.M. and H.L.M. performed experiments. X.C., D.F., Z.L., J.Z. and S.P., performed the bioinformatics analyses. E.M.P., X.C., J.E., S.P., J.R.D., R.C.R., G.P.Z. and J.Z. analyzed data. E.M.P., X.C., and R.C.R. prepared tables and figures. J.J. completed pathological evaluations. E.M.P., X.C., R.C.R. and G.P.Z. wrote the manuscript with contributions from C.R.G., B.C.F., M.D., A.P., J.Z. and J.R.D.

Competing financial interests

The authors declare no competing financial interests.

Accession codes

All whole-genome sequencing, whole-exome sequencing and transcriptome data have been deposited in the European Genome-phenome Archive (EGA), which is hosted by the European Bioinformatics Institute (EBI), under accession code EGAS00001000192.

[14]Department of Oncology, St. Jude Children's Research Hospital, Memphis, TN, USA

Abstract

Pediatric adrenocortical carcinoma is a rare malignancy with poor prognosis. Here we analyze 37 adrenocortical tumors (ACTs) by whole genome, whole exome and/or transcriptome sequencing. Most cases (91%) show loss of heterozygosity (LOH) of chromosome 11p, with uniform selection against the maternal chromosome. *IGF2* on chromosome 11p is overexpressed in 100% of the tumors. *TP53* mutations and chromosome 17 LOH with selection against wild-type *TP53* are observed in 28 ACTs (76%). Chromosomes 11p and 17 undergo copy-neutral LOH early during tumorigenesis, suggesting tumor-driver events. Additional genetic alterations include recurrent somatic mutations in *ATRX* and *CTNNB1* and integration of human herpesvirus-6 in chromosome 11p. A dismal outcome is predicted by concomitant *TP53* and *ATRX* mutations and associated genomic abnormalities, including massive structural variations and frequent background mutations. Collectively, these findings demonstrate the nature, timing and potential prognostic significance of key genetic alterations in pediatric ACT and outline a hypothetical model of pediatric adrenocortical tumorigenesis.

Adrenocortical tumors (ACTs) are rare[1]. A good outcome, as with most pediatric embryonal tumors, requires early diagnosis and complete surgical resection. Children with locally advanced or metastatic disease have a very poor prognosis, even with surgery and intensive chemotherapy[2].

Childhood ACT is often associated with germline *TP53* mutations (Li-Fraumeni syndrome, LFS)[3] or constitutional genetic and/or epigenetic alterations affecting chromosome 11p15 (Beckwith-Wiedemann syndrome, BWS)[4]. Both LFS and BWS have highly variable phenotypes, which include susceptibility to ACT and other embryonal malignancies[5]. The factors contributing to sporadic pediatric ACTs are unknown, although the similarity of these cases to those with a constitutional predisposition suggests a common mechanism of tumorigenesis[1].

ACT is uniquely amenable to molecular studies relevant to pediatric embryonal neoplasms in general. First, the marked clinical endocrine manifestations of ACT (e.g., virilization and Cushing syndrome) allow access to tumor tissue at an early disease stage. Second, ACT shares the epidemiological and molecular features of embryonal tumors[5]. Finally, a cluster of ACTs arising from a founder *TP53* mutation (R337H) in southern Brazil allows biologic, prognostic and therapeutic studies in a relatively large group of cases with a common predisposing factor[6–9].

Staging of pediatric ACT is based on tumor size and evidence of residual tumor after surgery[1]. Histopathologic classification criteria, which have been invaluable in distinguishing adenoma (benign) from carcinoma (malignant) in adult ACTs[10], have a limited role in guiding therapeutic decisions in pediatric ACTs, the great majority of which are classified as carcinomas or histology of undetermined malignant potential[11–12]. To advance our understanding of the initiation and progression of pediatric ACT, we undertook a comprehensive genomic analysis of 37 representative cases, including 12 tumors

associated with the germline *TP53*-R337H mutation, using a combination of whole genome sequencing (WGS), whole exome sequencing (WES) and transcriptome profiling (RNA-seq).

RESULTS

Clinical data

The clinical and biological characteristics of the 37 newly diagnosed ACT cases studied by WGS and WES are summarized in Supplementary Table 1a,b. The median age of the 25 girls and 12 boys at diagnosis was 53.5 months (range, 9.7 to 184.7 months). Tumors were sporadic (n=10) or associated with constitutional cancer predisposition conditions [Brazilian founder *TP53*-R337H (n=12); other types of germline *TP53* mutations (n=13) and BWS (n=2)] and included 29 carcinomas, 3 adenomas, and 5 tumors of undetermined malignant potential. These cases were selected on the basis of availability of paired tumor and germline samples and isolation of high-quality tumor DNA. Although treatment was not uniform, it generally adhered to the Children's Oncology Group (COG) ARAR0332 protocol[1], consisting of surgery alone for stage I and II disease, and surgery followed by intensive chemotherapy (cisplatin, doxorubicin, etoposide and mitotane) for advanced-stage (III and IV) disease. At a median follow-up of 38 months, 11 of 35 (31%) patients had experienced an adverse event (relapse or death). Five of these 11 had died of progressive disease at the time of this report, and six remain alive in second complete remission. Two patients were lost to follow-up. Clinical data from 34 additional ACT patients studied as an independent comparison group ("convenience cohort") is included in Supplementary Table 1c.

Genome and transcriptome analyses

Primary ACTs and matched peripheral blood DNA were analyzed by WGS (n=19) at an average 41.9X coverage (Supplementary Table 2a) or by WES (n=18) at an average 84.8X coverage (Supplementary Table 2b) (Pediatric Cancer Genome Project (PCGP), http://pcgpexplore.org/). All genetic lesions, including single nucleotide variations (SNV), small insertions/deletions (indels) and structural variations (SVs) were experimentally validated (Supplementary Fig. 1). In the WGS samples, the median number of non-silent point mutations was 5 (range, 1–97), median background mutation rate (BMR) was 3.78×10^{-7} (range, 5.01×10^{-8} to 2.40×10^{-6}) and median number of SVs per case was 61 (range, 0–812) (Supplementary Table 3a–d). Transcriptome profiles of normal adrenocortical tissue (n=6) and ACT samples from the WGS cohort (n=16) were analyzed by RNA sequencing (RNA-seq) (Supplementary Table 2c).

TP53 mutations

Germline *TP53* mutations were present in 25 of the 37 patients (68%) in the combined WGS and WES cohorts, 12 of which were the Brazilian founder R337H mutation (Fig. 1a and Supplementary Fig. 3a). Somatic mutations (R175H, R273C, and a homozygous deletion of ~200 Kb of chromosome 17 encompassing *TP53*) were also identified in 3 of the 12 ACTs associated with wild-type germline *TP53* (Supplementary Figs. 3a,b).

Sanger sequencing identified germline *TP53* mutations in 11 of 34 cases (32%) in the independent comparison cohort (Supplementary Table 1c). Of the 23 ACTs in this group associated with germline wild-type *TP53*, three tumors acquired a *TP53* mutation (c. 134_135 insT, E180K and R273H) (Supplementary Fig. 4a).

Somatic *ATRX* mutations

ATRX encodes a helicase that functions in chromatin remodeling and telomere structural maintenance, and it cooperates with *DAXX* to incorporate the histone variant H3.3 into chromatin[13]. *ATRX* somatic nonsense mutations and SVs deleting multiple exons were identified by WGS in 6 of 19 ACTs (32%), all of which were associated with germline *TP53* mutations (Figs. 1a and 2a,b). An *ATRX* somatic missense mutation (R2164S) was also identified by WES in the case with somatic homozygous deletion of *TP53* (Fig. 2a and Supplementary Fig. 3b). No mutations were detected in the coding region of *DAXX* or *TERT* by WGS or WES. Furthermore, no mutations were identified in the *TERT* core promoter by targeted Sanger sequencing. Although broad regional amplification encompassing the *TERT* locus was observed in 13 of the 19 WGS cases (68%), no *TERT* expression was detected by RNA-seq.

WGS-based telomere length analysis showed an increase of telomeric DNA in all 6 tumors with *ATRX* mutations, but not in tumors with wild-type *ATRX* ($P = 3.7 \times 10^{-5}$, Fisher's exact test) (Fig. 2c). Telomere FISH analysis of 22 available formalin-fixed, paraffin-embedded tumor specimens revealed large, ultra-bright telomere foci (Fig. 2d) in cases harboring *ATRX* mutations (n=5)**,** suggesting the activation of an alternative lengthening of telomeres (ALT) mechanism. Telomere foci were also observed in the SJACT023 tumor, although WES did not detect an *ATRX* mutation.

Somatic β-catenin mutations

Somatic β-*catenin* (*CTNNB1*) mutations were identified in 3 of the 37 (8%) tumors analyzed in the combined WGS and WES cohorts (Fig. 1a and Supplementary Fig. 5). Targeted Sanger sequencing of *CTNNB1* exon 3 revealed 10 additional somatic mutations in 34 pediatric ACTs in the independent comparison cohort (Supplementary Fig. 4b). Overall, *CTNNB1* mutations (n=13) were detected only in tumors with wild-type germline *TP53* (n=35) and not in those with constitutional *TP53* mutations (n=36) ($P = 2.5 \times 10^{-5}$, Fisher's exact test). However, three tumors with somatic *CTNNB1* mutations had also acquired a *TP53* mutation (IPACTR001, IPACTR013 and IPACTR019) (Supplementary Fig. 4b and Supplementary Table 1c).

Genomic classification of ACT

WGS defined three groups of pediatric ACT based on the mutational status of *TP53* and *ATRX*: Group 1) germline *TP53* and somatic *ATRX* mutations (n=6); Group 2) germline *TP53* mutations and no *ATRX* mutation (n=9); and Group 3) both wild-type *TP53* and *ATRX* (n=4) (Fig. 1a). Group 1 cases had significantly greater tumor weight ($P = 0.007$, Mann-Whitney test), were significantly more likely to have stage 3 or 4 disease ($P = 0.020$, Kendall test), and had poorer event-free survival than Groups 2 and 3 ($P = 5.0 \times 10^{-5}$, exact log rank test) (Fig. 1a,b). Group 1 ACTs also had a significantly larger number of SVs ($P =$

0.021, Mann-Whitney test) and higher background mutation rate (BMR) ($P = 0.015$, Mann-Whitney test) (Supplementary Fig. 3c). In addition, these tumors showed significantly higher expression of genes associated with chromosome instability and deregulation of cell cycle control (*PTTG1*, $P = 0.019$; *ESPL1*, $P = 0.015$; *CCNB1*, $P = 0.018$; *BUB1*, $P = 0.023$; *TPX2*, $P = 0.032$; and *MCM2*, $P = 0.040$, t-test) (Fig. 1a). Although all cases in Group 2 carried germline *TP53* mutations (8 of 9 cases had the founder R337H mutation and were diagnosed in southern Brazil), they displayed variable clinical findings. Group 2 patients with the R337H mutation were young (median age, 30 months), exhibited signs of virilization and had relatively small tumors [median tumor weight 68 g vs 585 g in Group 1 ($P < 0.006$, Wilcoxon rank sum test)]. These tumors showed variable numbers of SVs and BMR, and variable expression of selected target genes (Fig. 1 and Supplementary Fig. 3c). A distinguishing feature of this group is the lack of *ATRX* mutations and the shortening of telomeres as compared to Group 1. Group 3 tumors showed a relatively small number of SVs and a low BMR, and gene expression of those selected genes was similar to that in normal adrenocortical tissue, consistent with their more favorable outcome (Fig. 1 and Supplementary Fig. 3c).

WGS did not reveal any specific genetic alterations that distinguished ACTs harboring the founder *TP53*-R337H from tumors with other *TP53* mutations. However, R337H tumors that had acquired an *ATRX* mutation (cases SJACT062 and SJACT069) clustered in Group 1 and exhibited an aggressive phenotype (Figs. 1 and 3). The remaining 8 R337H cases showed variable molecular profiles and disease stage (Fig. 1 and Supplementary Fig. 2). Figure 3 illustrates the relationship among histopathological features, tumor weight, stage and complexity of genomic abnormalities for four cases with the same predisposing *TP53*-R337H germline mutation.

Loss of heterozygosity of chromosomes 11 and 17

Chromosome 17 loss of heterozygosity (LOH) was observed in 28 of 37 ACTs (76%) by WGS and WES. All tumors with germline (n=25) and somatic (n=3) *TP53* mutations underwent LOH with selection against the wild-type allele (Supplementary Fig. 2). More specifically, WGS demonstrated copy-neutral LOH (cn-LOH) of the entire chromosome 17 in all tumors associated with germline *TP53* mutations (n=15), as well as in two (SJACT003, SJATC004) of the four cases with wild-type *TP53* (Supplementary Fig. 2).

Chromosome 11p LOH was also identified in 32 of the 35 ACTs (91%). Two BWS patients (SJACT009 and SJACT065) with germline 11p homozygosity, indicative of uniparental disomy (UPD), were excluded from the analysis as LOH could not be assessed (Supplementary Fig. 2 and Fig 4a). Furthermore, cn-LOH of chromosome 11p was demonstrated by WGS in 14 of the 18 informative ACTs (Supplementary Fig. 2). Microsatellite marker analysis of an additional 22 pediatric ACT cases from our independent comparison cohort revealed chromosome 11p LOH in 20 tumors (95%, as IPACTR004 was excluded due to UPD) (Supplementary Fig. 4c). Remarkably, 100% of the cases from the combined cohorts that underwent chromosome 11p15 LOH and had available parental DNA (n=23) selectively retained the paternal chromosome ($P = 2.4 \times 10^{-7}$, sign test) (Fig. 4a and Supplementary Fig. 4c).

Human chromosome 11p15 contains a large cluster of imprinted genes, including *IGF2*, *CDKN1C*, *KCNQ1* and *H19. IGF2* is a paternally expressed fetal growth factor, whereas the cell cycle inhibitor *CDKN1*C (p57), potassium channel protein *KCNQ1* and the non-coding *H19* transcripts are expressed from the maternal allele. Expression of genes localized at 11p15 (chr11:1704500-3658789) was analyzed by transcriptome profiling. RNA-seq confirmed greater expression of *IGF2* in all tumors in the WGS cohort compared to normal adrenocortical tissue ($P = 2.987 \times 10^{-7}$, t-test) (Supplementary Fig. 6). Expression of *KCNQ1*, *CDKN1C* and *H19* was low in most cases, consistent with loss of the maternal chromosome 11p. SJACT006, which retained both parental copies of chromosome 11, also displayed elevated *IGF2* expression and deregulation of maternally expressed genes, suggesting a loss of imprinting control at this locus (Supplementary Fig. 6).

Timing of cn-LOH of chromosomes 11 and 17

To infer the temporal order of somatic SNV acquisition and cn-LOH in chromosomes 11 and 17, we compared the mutant allele fractions (MAFs) of SNVs in cn-LOH regions to allelic imbalance (AI) values, which express the different mutant allele fractions (germline heterozygous SNPs) in tumor vs. germline samples (Figs. 4b,c and Supplementary Fig. 7). A cn-LOH event in the tumor cells will lead to an expected AI value of 0.5. Similarly, somatic SNVs acquired before cn-LOH would result in either a homozygous reference allele (R) or a homozygous mutant (M) allele, while SNVs accumulated after cn-LOH would remain heterozygous in the absence of a second hit (Supplementary Fig. 7a). Our analysis of 14 informative WGS samples demonstrated that most SNVs in chromosomes 11p and 17p were acquired after cn-LOH, although SJACT005 underwent cn-LOH during SNV accumulation (Figs. 4b,c and Supplementary Fig. 7b). These findings indicate that cn-LOH of chromosomes 11p and 17p occurs early in adrenocortical tumorigenesis and precedes the accumulation of SNVs in these regions.

Chromosomal integration of human herpesvirus-6

Human herpesvirus-6 (HHV6) was detected by WGS in the germline and tumor DNA of SJACT004 (Fig. 5a) and by Sanger sequencing in SJACT017. FISH analysis confirmed the site of chromosomal integration of HHV6 as the telomeric region of 11p in both cases (Fig. 5b). PCR analysis demonstrated paternal transmission of chromosomally integrated HHV6 in SJACT017 (Fig. 5c). Microsatellite marker analysis and WGS confirmed chromosome 11 LOH with retention of integrated HHV6 in both cases (Supplementary Fig. 2, Fig. 4a and Supplementary Fig. 4c). Genomic and transcriptome analyses of SJACT004 identified few somatic SNVs and SVs, but showed elevated *IGF2* expression (Supplementary Figs. 2 and 6). Both ACTs were small, stage 1 tumors and with good prognosis (Supplementary Table 1a,b).

Other genetic events

Chromosomal copy number alterations (CNA) were also assessed by a modified version of GISTIC (genomic identification of significant targets in cancer). Deletion of chromosome 4q34 was observed in 11 of 19 tumors (58%) (Supplementary Fig. 8a,b). The most

commonly deleted region overlapped a 5 Mb area encompassing *LINC00290* (long intergenic non-protein coding RNA 290)[14].

Chromosomal copy number gains were widespread with 9q being overrepresented and amplified in 16 of 19 WGS ACTs, similar to previously reported findings (Supplementary Fig. 8a,c)[14]. Chromosome shattering consistent with chromothripsis[15] (Supplementary Fig. 9) and patterns of localized hypermutation (kataegis[16]) (Supplementary Fig. 10) were observed in late stage tumors (Fig. 1a). Structural variants resulting in the expression of fusion genes were infrequent and non-recurrent (Supplementary Table 4).

DISCUSSION

Our genomic findings define cn-LOH of chromosome 11p, with selection against the maternal chromosome and consequent *IGF2* overexpression, as an early event and a hallmark of pediatric adrenocortical tumorigenesis.

Although pediatric ACT is strongly associated with germline *TP53* mutations[17–19] (60–70% of children with ACT[3]), only 4–6% of carriers develop adrenocortical tumors[1], suggesting the involvement of cooperating genetic alterations. We propose that germline *TP53* mutations may contribute to adrenocortical tumorigenesis by promoting chromosomal instability[20,21]. In this setting, aneuploid adrenocortical cells that experience chromosome 11p LOH and deregulation of imprinted genes on 11p15 may be selected and expanded via constitutive overexpression of *IGF2*, which encodes a potent mitogen and fetal growth-promoting protein[22,23]. This mechanism is consistent with chromosome 11p abnormalities and *IGF2* overexpression in all cases of ACT with germline *TP53* mutations. Clones that undergo chromosome 17 LOH and lose wild-type *TP53*, become more unstable, accumulate additional SNVs and are selected for further expansion. In support of this hypothesis, our temporal studies place cn-LOH of chromosomes 11p and 17 during early tumorigenesis, before the acquisition of widespread genomic alterations.

Our WGS study included 10 Brazilian cases with the founder *TP53*-R337H mutation, which could influence the resulting genomic landscape findings. *TP53*-R337H is a missense mutation that is partially functional[6,24]; hence, we expected that genomic changes could be different from those with nonfunctional mutations. Our genomic studies showed that some cases with the R337H mutation had secondary genetic events that were similar to those seen with other types of *TP53* mutations, such as concomitant cn-LOH of chromosomes 11 and 17p early during tumorigenesis, as well as the deregulation of *IGF2* expression and acquired *ATRX* mutations. These findings are consistent with those from high-density SNP analysis that demonstrated the pattern of gains and losses is similar in pediatric ACTs with R337H and other *TP53* mutations[14]. However other cases with R337H mutations had much simpler genomes similar to those with wild type *TP53*. It is possible that secondary genomic changes increase with time from tumor initiation to diagnosis. Alternatively other genetic constitutional or acquired changes account for the observed heterogeneity observed in cases with the R337H mutations. Further studies will be required to examine these possibilities.

LOH of chromosome 11p15 and genomic imprinting abnormalities within this region that lead to constitutive *IGF2* expression are features of many other pediatric tumors, including rhabdomyosarcoma[25], Wilms tumor[26], and hepatoblastoma[27]. Similarly, adult adrenocortical carcinomas, but not adenomas, show genomic imprinting abnormalities at chromosome 11p15[28,29]. However, transgenic mouse models demonstrate that *IGF2* overexpression is not by itself sufficient to promote adrenocortical tumorigenesis[30] but must cooperate with other genetic alterations, such as activation of β-catenin[31]. Consistent with these findings, *CTNNB1*-activating mutations were relatively frequent in our cohort, particularly in cases with germline wild- type *TP53*.

Assié and collaborators recently reported the characterization of 45 adult adrenocortical carcinomas (ACC) using an integrated genomic analysis approach[29]. A comparison of our findings to this published study highlights similarities and differences in the genetic changes that occur in pediatric and adult ACTs (Supplementary Table 5). Remarkably, 11p15 LOH involving the *IGF2* locus was observed in both pediatric ACT (91%) and adult ACC (82%), underscoring the critical role of deregulated *IGF2* expression in adrenal cortex tumorigenesis. Aneuploidy with widespread chromosomal gains (e.g., chromosome 19) and deletions (e.g., 4q34.3) was also observed in both pediatric and adult cases. However, amplification of chromosome 9q, a region that includes *NOTCH1* and *NR5A1* (*Steroidogenic Factor-1*), occurred in 90% of pediatric ACTs (Supplementary Fig. 8a,c), but not in adult ACC[29]. Activating mutations in *CTNNB1* were common to both pediatric and adult ACT, but additional mutations within the Wnt/β-catenin signaling pathway, in particular *ZNRF3*, were only observed in adult tumors. Germline *TP53* mutations were predominantly associated with pediatric ACT, whereas somatic *TP53* mutations were relatively infrequent in both groups. The alternative lengthening of telomeres (ALT phenotype) was associated with *DAXX* or *ATRX* mutations in adult tumors, but exclusively with *ATRX* mutations in pediatric cases. Amplification of *TERT* was common in both groups, but no *TERT* mutations were detected in the pediatric cases, consistent with the absence of *TERT* expression.

A lack of strong prognostic indicators has limited progress in the management of childhood ACT. Overall event-free survival is only about 50%, and patients with advanced-stage disease have very poor overall survival[1,2]. Unlike studies of other pediatric embryonal tumors[32–34], histopathological examination[11] and molecular findings[35] in pediatric ACT has not produced relevant prognostic categories or novel treatment approaches. Tumor weight, volume and surgical resectability form the basis of the current Children's Oncology Group (COG) disease-stage classification[1]. However, this system needs improvement, as many patients experience relapse despite small, completely excised tumors while others are cured despite histological findings suggestive of carcinoma[36].

Our genomic analysis opens opportunities to improve the current tumor size- histology-disease stage prognostic scheme for pediatric ACT[1–2]. Notably, tumors with both germline *TP53* and somatic *ATRX* mutations (Group 1) were significantly associated with high tumor weight, advanced disease (COG stage III/IV), and poor event-free survival. SJACT069 (R337H) exemplifies such a case; it was staged as limited disease (COG stage II) and initially managed with surgery alone, but later metastasized to the lungs. Moreover, 5 of 6

patients in Group 1 had adverse events (relapse or death), consistent with the genomic findings indicative of an aggressive phenotype. Cases with germline *TP53* mutations and wild-type *ATRX* (Group 2) are clinically and molecularly heterogeneous. Although all cases in this group carried *TP53* mutations (8 of 9 cases harbor the founder R337H), they had fewer genomic abnormalities, smaller tumors and generally much better clinical outcome than cases in Group 1. It is not surprising that patients in southern Brazil with the R337H mutation were diagnosed earlier, as pediatricians there are familiarized with the first signs of ACT and promptly refer these children for treatment. However, three patients (one with the *TP53* G245C and two with the Brazilian R337H mutation) overexpressed genes associated with chromosome instability and cell cycle control (Fig 1a; Supplementary Table 1). The two cases with R337H required chemotherapy because of advanced stage disease in one and tumor rupture in the other. The patient with the G245C, a child more than 10 years of age at diagnosis of ACT, had delayed diagnosis of a very large tumor in the absence of endocrine signs (a “non-functional” tumor). This child was treated with surgery followed by chemotherapy, but eventually died of relapsed disease. These observations suggest that pediatric *TP53*-associated tumors arise from a simpler genomic background (adenoma or undetermined malignant potential) and progress to acquire complex and unstable genomic aberrations (carcinoma). The results of newborn screening for the *TP53* mutation in Brazil and surveillance of carriers for early signs of ACT[9] are consistent with this concept[37]. Finally, ACTs with wild-type *TP53* exhibit relatively simple genomes and despite their large size in some cases, patients generally have a good outcome. Because of the small number of these cases, additional genomic studies will be needed to clarify the role of molecular changes in this subset of patients.

In two of our cases (SJACT004 and SJACT017), HHV6 was selectively integrated into the telomeric region of chromosome 11p. HHV6 is known to integrate into the genome at a low frequency (~1%), preferring the telomeric regions of chromosomes 9q, 11p, 17p, and 19q[38,39]. A recent report documented the role of integrated HHV6 in disrupting telomeres, leading to selective aneuploidy[40]. Whether chromosomal integration of HHV6 facilitates 11p cn-LOH and deregulation of imprinting at the 11p15 locus, leading to *IGF2* overexpression remains to be determined.

In summary, our study identified key genetic alterations and their temporal relationships in pediatric adrenocortical tumorigenesis. The genomic complexity of childhood ACTs, particularly those with both germline *TP53* and acquired *ATRX* mutations, may explain the failure of standard chemotherapy, underscoring the importance of early diagnosis and improved prognostic classification.

METHODS

Patients and samples

Written informed consent was obtained from parents or legal guardians for inclusion in the St. Jude Children’s Research Hospital (St. Jude) International Pediatric Adrenocortical Tumor Registry (IPACTR) (http://clinicaltrials.gov/show/NCT00700414) or for participation in Children’s Oncology Group (COG) ARAR0332 protocol (http://clinicaltrials.gov/show/NCT00304070). IPACTR registers childhood cases of ACT

worldwide. COG studies enroll patients from the U.S., Canada, and southern Brazil, where 90% of cases carry the founder *TP53*-R337H mutation. Diagnosis was made on the basis of the gross and histologic appearance of tissue obtained at surgery. The diagnosis of adrenocortical tumor was centrally reviewed and confirmed. Tumors were further classified as adenoma (benign), carcinoma (malignant) or having histology of undetermined malignant potential. No attempt was made to obtain individual tumor scores.

Samples for WGS (n=19) and WES (n=18) included matched peripheral blood and primary tumor tissue from 26 IPACTR patients and 11 COG patients. An additional group of 34 IPACTR patients with matched primary tumor and blood samples, and blood-derived DNA from 23 sets of parents, were included for analysis of chromosome 11p LOH, *TP53* and *CTNNB1* mutation. Six samples of normal adrenocortical tissue obtained during nephrectomy for Wilms tumor were used as controls in gene expression studies as well 16 tumor samples studied in WGS cohort. All tumor samples underwent estimation of the purity-adjusted MAF, tumor purity, and tumor heterogeneity and quantitative analysis of chromothripsis[41].

Tumor Purity Estimations

For germline heterogeneous SNPs, loss of heterozygosity (LOH) measures the absolute difference between the mutant allele fraction in tumor and that in germline sample (0.5). LOH is the result of copy number alterations and/or cn-LOH in tumor cells. Compared to copy number gains (a single copy gain in 100% tumor results in a LOH value of 0.167), regions with copy number loss showed stronger LOH (a single copy loss in 100% tumor result in a LOH value of 0.5). Consequently, we used LOH signals in copy neutral or heterozygous copy number loss regions (CNA value between [−1, 0]) to estimate tumor purity for all WGS samples. Briefly, a single copy loss in *x*% tumor cells resulted in an estimated CNA value of $-\frac{x}{100}$ and a LOH value of $\frac{x}{400-2x}$. Assuming the remaining LOH signal came from cn-LOH (cn-LOH in *x*% tumor cell resulted in a LOH value of $\frac{x}{200}$), the tumor content in a region could be estimated as the sum of the fraction with copy number loss and the fraction with cn-LOH by: $-CNA+2*\left(LOH-\frac{-CNA}{4+2CNA}\right)$. Using tumor content estimates from various regions within the genome, we performed an unsupervised clustering analysis using the *mclust* package (version 3.4.8) in R (version 2.11.1). The tumor purity of the sample was defined as the highest cluster center value among all clusters.

Purity Adjusted Mutant Allele Fraction (MAF) Estimation

MAF for validated SNVs was estimated as $\frac{\#Mutant\ reads}{(\#Total\ reads)\times(tumor\ purity)}$ using deep sequencing data.

Tumor Heterogeneity Estimation

We used all validated autosomal SNVs satisfying the following criteria in heterogeneity analysis:

1. In copy neutral region (Log2ration between (−0.1, 0.1) in CNV analysis).
2. Not in regions with LOH (LOH value < 0.1).
3. With MAF > 0.05 or mutant allele count > 2.

We drew the kernel density estimate plot for MAFs of the qualifying SNVs using the *density* function in the *stat* package in R. We also estimated the number of significant peaks and the relative MAF component for each peak (peaks with less than 5 SNVs, peaks with less than 1% SNVs, and peaks with excessive variance were ignored). A sample with heterogeneity shows density peaks at a MAF smaller than 0.5 (the expected MAF assuming heterogeneous SNVs).

Kataegis Analysis

Kataegis analysis was performed on all validated Tier1–3 SNVs and SV breakpoints for each sample. The intermutation distance for a SNV was calculated as the distance to its nearest neighbor. For each SNV, its distance to the nearest validated SV breakpoint was also calculated. We defined microclusters of kataegis as clusters that contain at least 5 consecutive SNVs with inter-variant distance less than 10 kb. Mutant allele frequency (MAF) was estimated for SNVs with at least 20× coverage in tumor BAMs based on deep sequencing of custom capture validation.

This study was approved by the St. Jude Institutional Review Board and by the Cancer Therapy Evaluation Program of the National Cancer Institute (ARAR12B1).

Whole genome sequencing

WGS was performed as previously described[42,43]. WGS mapping, coverage, quality assessment, SNV, indel detection, tier annotation for SNVs, prediction of deleterious effects of missense mutations, and identification of LOH have been described previously[42]. SVs were analyzed by using CREST software and annotated as previously described[42,44]. The reference human genome assembly NCBI Build 37 was used for mapping samples. CNAs were identified by comparing read depth in tumor vs. matched normal samples and using a novel algorithm, CONSERTING (COpy Number SEgmentation by Regression Tree In Next-Gen sequencing).

SNVs were classified according to the following three tiers, as previously described[42].

Tier 1: Coding synonymous, nonsynonymous, and splice-site variants and non-coding RNA variants

Tier 2: Conserved variants (cutoff conservation score ≥ 500, based on either the phastConsElements28way table or the phastConsElements17way table from the UCSC genome browser [http://genome.ucsc.edu/] and variants in regulatory regions annotated by UCSC annotation [regulatory annotations included targetScanS, ORegAnno, tfbsConsSites, vistaEnhancers,eponine, firstEF, L1 TAF1 Valid, Poly(A), switchDbTss, encodeUViennaRnaz, laminB1, and cpgIslandExt])

Tier 3: Variants in non-repeat masked regions.

Tier 4: All other SNVs.

Exome sequencing

For exome sequencing, DNA libraries were prepared from 1 μg of whole genome– amplified (WGA) DNA from matched samples by using the Illumina TruSeq DNA library prep kit according to the manufacturer's protocol. The quality of library construction was assessed on an Agilent Bioanalyzer. Germline and diagnostic library samples were independently pooled for exome capture by using the Illumina TruSeq Exome Enrichment kit as instructed by the manufacturer. Captured libraries were then clustered on the Illumina c-bot and sequenced on an Illumina HiSeq 2000 platform by conducting 100 base pair–end multiplexed reads at an equivalent of 3 samples per lane.

Sequence validation

To enrich regions containing putative sequence alterations, genomic coordinates of the WGS targets were used to order Nimbelgen Seqcap EZ solution bait sets (Roche). Library construction and target enrichment were performed per the manufacturer's instructions, using repli-G (Qiagen) WGA DNA. Enriched targets were sequenced on the Illumina platform by paired-end 100-cycle sequencing. The resulting data were converted to FASTQ files by using the CASAVA 1.8.2 (Illumina) program and mapped with a Burrows-Wheeler Aligner before pipeline analysis. Putative SNVs and indels from exon sequencing were validated by next-generation amplicon sequencing. Briefly, primers were designed for genomic regions (hg19) flanking the detected SNV but no nearer than 100 base pairs. PCR was performed by using 20 to 30 ng of WGA DNA from each sample. DNA from diagnostic tumor samples and matched germline samples was used for each primer set to confirm the presence of the SNV/indel in the diagnostic sample. Standard PCR was performed in 25-μl reactions, using Accuprime GC-rich DNA polymerase (Invitrogen) with the following reaction conditions: 95°C for 3 min; 35 cycles of 95°C for 30s, 65°C for 30s, and 72°C for 1 min; and a 72°C 10 min extension with cooling to 4°C. All PCR amplicons were verified on a 2% E-gel (Invitrogen) to ensure single amplified products.

Transcriptome sequencing

For library construction, 2–5 μg of total RNA was extracted from tumor samples by using Qiagen RNeasy Mini kits according to the manufacturer's instructions. RNA concentration was measured by using a NanoDrop 100 Spectrophotometer (Thermo Scientific). RNA integrity was measured by using an Agilent Technologies 2100 Bioanalyzer Lab-on-a-chip system. Total RNA was treated with DNAse I (Invitrogen) and enriched for poly A containing mRNA using oligo dT beads (Dynabeads, Invitrogen). The cDNA synthesis used random hexamers and the Superscript Double- Stranded cDNA Synthesis kit (Invitrogen). Paired-end reads from mRNA-seq were aligned to the following 4 database files by using a Burrows-Wheeler Aligner (0.5.5)[45] (i) human NCBI Build 37 reference sequence, (ii) RefSeq, (iii) a sequence file representing all possible combinations of non-sequential pairs in RefSeq exons, and (iv) AceView database flat file downloaded from UCSC, representing transcripts constructed from human expressed sequence tag (EST). The mapping results from databases (ii)–(iv) were aligned to human reference genome coordinates. The final

BAM file (compressed binary version of the Sequence Alignment/Map [SAM] format) file was constructed by selecting the best alignment in the four databases. RNA expression level was measured by fragments per kilobase of transcript per million fragments mapped (FPKM)[46]. SVs were detected by using the CIRCERO algorithm, a novel algorithm that uses *de novo* assembly to identify structural variation in RNA-seq data (unpublished data). The structural variants detected in RNA-seq data were validated with MiSeq sequencing. Primer pairs were designed (with Primer3) to bracket the genomic regions containing putative structural variations. The structural variations found by RNA-seq are reported in Supplementary Table 4.

GISTIC analysis

We used cghMCR (an R implementation of a modified version of GISTIC analysis[47]) to find regions that contained copy number alterations. We identified significantly amplified genes as those with segments of gain or loss (SGOL) scores 3 standard deviations above the mean SGOL scores of all “gains”. Genes with SGOL scores 3 standard deviations below the mean SGOL scores of all “losses” were selected as significantly deleted genes.

Timing of cn-LOH

The cn-LOH regions were estimated from the CNA and LOH analysis data. When cn- LOH was identified in a pure tumor cell population, heterozygous alleles had become homozygous for either the reference allele or the alternative allele. Consequently, the mutant allele fraction for SNVs accumulating before cn-LOH was either 0 (homozygous reference allele) or 1 (homozygous alternative allele), while SNVs occurring after cn- LOH had a maximum MAF of 0.5 (assuming no second mutation at the same locus) in tumor cells. We inferred the temporal order of cn-LOH and SNV accumulation in a genomic segment by comparing the allelic imbalance values with the region’s MAF.

Telomeric DNA content and telomere FISH

The WGS data were analyzed for total telomeric DNA content in tumors and matched germline DNA in 19 cases. Telomeric content reads containing (TTAGGG)4 or (CCCTAA)4 were counted and normalized to the average genomic coverage, and the log2 ratio of diagnostic and germline telomeric content estimates was then calculated to allow classification of telomeric content as gain, no change, or loss[48]. Telomere FISH was performed on available formalin-fixed, paraffin-embedded tissue samples (n=22) from the WGS and WES cohorts. Interphase FISH was performed on 4-μm-thick, formalin-fixed, paraffin-embedded tissue sections. The Cy3-labeled TelG probe (PNAbio) was co-denatured with the target cells on a hotplate at 90°C for 12 min. The slides were incubated for 48 h at 37°C and then washed in 4 M urea/2X SSC at 45°C for 5 min. Nuclei were counterstained with 200 ng/mL of 4′, 6-diamidino-2-phenylindole (Vector Laboratories). The telomeric probe (red) hybridizes to telomeres on all chromosomes; a probe for 4p (green) was used as control.

Analysis of microsatellite markers on chromosome 11p

To identify commonly deleted regions on chromosome 11p15, we assessed LOH in 16 paired normal and tumor DNAs selected from the recurrence groups (WES) and in 22 additional IPACTR cases. We included peripheral blood DNA from 23 pairs of parents. Genomic DNA was extracted by using standard protocols. Fluorescence PCR semi-automated genotyping was used to detect and analyze allelic losses by using a panel of 5 microsatellite markers (D11S1363, D11S922, D11S4046, HUMTH01 and D11S988).

TP53 and *CTNNB1* mutations

To detect and validate *TP53* and *CTNNB1* mutations, genomic DNA from ACT samples was tested by PCR-based bi-directional DNA sequencing of exons 2–11 and intron-exon boundaries for *TP53* and exon 3 (codons 5–70) for *CTNNB1*. Sequencing reactions were carried out on a high-throughput 3730xl DNA Analyzer (Applied Biosystems).

TERT core promoter mutational status

The *TERT* core promoter (HG19 coordinates, chr5: 1295151-1295347) was amplified in 19 pediatric ACT by PCR. Briefly, 10–20 ng of sample DNA was added to a 25 ul reaction containing amplitaq gold 360 master mix (Applied Biosystems) with 400 nM each of amplification primers [5′- CAGCGCTGCCTGAAACTCG-3′ (sense) and 5′-CCACGTGGCGGAGGGACT-3′ (antisense)] resulting in a PCR product of 197 bp. Sequencing reactions were carried out on a high-throughput 3730xl DNA Analyzer (Applied Biosystems).

HHV-6 chromosomal integration

We amplified the sequences of the HHV6 major capsid protein and *U94* genes in tumor and blood DNA from cases in the WGS and WES cohorts (n=37). PCR and cycling conditions followed a previously described protocol[49–50]. Cases positive by PCR were tested by FISH analysis. Peripheral blood mononuclear cells were cultured for 72 h in RPMI 1640 containing 20% FCS and 10 μg/ml PHA. After 1.0 h of colcemide treatment, cells were harvested according to standard cytogenetic techniques. Cells in metaphase were examined by FISH using HHV6 cosmid probes labeled by nick translation with fluorescein-dUTP and a dual-color probe mapped to the sequences 5′ and 3′ of the common breakpoint region within the *MLL locus* (11q23) (Abbott Molecular). The HHV6/*MLL* probe mixture was applied to target metaphases and incubated at 37 °C overnight. After the slide was washed with 2X SSC, 10 μl of DAPI counterstain was applied to the target area for visualization.

Supplementary Material

Refer to Web version on PubMed Central for supplementary material.

Acknowledgments

We thank the St. Jude Children's Research Hospital Hartwell Center, Tissue Resources Core Facility, Marc Valentine and the Cytogenetics Laboratory, and Pathology Department for expert assistance and Drs. Charles Mullighan, Kathryn Roberts and Evan Parganas for assistance with figures. We thank Drs. Gad B. Kletter, Andres Yunes and Ana Luisa Seidinger for clinical samples. We thank Sharon Naron for scientific edition. This work was supported by Cancer Center Support grant CA21765 and grants EY014867, EY018599, and CA168875 (M.A.D)

from the National Institutes of Health and by the American Lebanese Syrian Associated Charities (ALSAC). Whole-genome sequencing was supported as part of the St. Jude Children's Research Hospital–Washington University Pediatric Cancer Genome Project. M.A.D.is a Howard Hughes Medical Institute Investigator.

References

1. Ribeiro RC, Pinto EM, Zambetti GP, Rodriguez-Galindo C. The International Pediatric Adrenocortical Tumor Registry initiative: contributions to clinical, biological, and treatment advances in pediatric adrenocortical tumors. Mol Cell Endocrinol. 2012; 351:37–43. [PubMed: 22040600]
2. Michalkiewicz E, et al. Clinical and outcome characteristics of children with adrenocortical tumors: a report from the International Pediatric Adrenocortical Tumor Registry. J Clin Oncol. 2004; 22:838–845. [PubMed: 14990639]
3. Wasserman JD, Zambetti GP, Malkin D. Towards an understanding of the role of p53 in adrenocortical carcinogenesis. Mol Cell Endocrinol. 2012; 351:101–110. [PubMed: 21930187]
4. Weksberg R, Shuman C, Beckwith JB. Beckwith-Wiedemann syndrome. Eur J Hum Genet. 2010; 18:8–14. [PubMed: 19550435]
5. Steenman M, Westerveld A, Mannens M. Genetics of Beckwith-Wiedemann syndrome-associated tumors: common genetic pathways. Genes Chromosom Cancer. 2000; 28:1–13. [PubMed: 10738297]
6. Ribeiro RC, et al. An inherited p53 mutation that contributes in a tissue-specific manner to pediatric adrenal cortical carcinoma. Proc Natl Acad Sci USA. 2001; 98:9330–9335. [PubMed: 11481490]
7. Latronico AC, et al. An Inherited Mutation Outside the Highly Conserved DNA-Binding Domain of the p53 Tumor Suppressor Protein in Children and Adults with Sporadic Adrenocortical Tumors. J Clin Endocrinol Metab. 2001; 86:4970–4973. [PubMed: 11600572]
8. Pinto EM, et al. Founder effect for the highly prevalent R337H mutation of tumor suppressor p53 in Brazilian patients with adrenocortical tumors. Arq Bras Endocrinol Metabol. 2004; 48:647–650. [PubMed: 15761534]
9. Custódio G, et al. Impact of neonatal screening and surveillance for the TP53 R337H mutation on early detection of childhood adrenocortical tumors. J Clin Oncol. 2013; 31:2619–2626. [PubMed: 23733769]
10. Lau SK, Weiss LM. The Weiss system for evaluating adrenocortical neoplasms: 25 years later. Human Pathology. 2009; 40:757–768. [PubMed: 19442788]
11. Dehner LP, Hill DA. Adrenal cortical neoplasms in children: why so many carcinomas and yet so many survivors? Pediatr Dev Pathol. 2009; 12:284–291. [PubMed: 19326954]
12. Michalkiewicz EL, et al. Clinical characteristics of small functioning adrenocortical tumors in children. Med Pediatr Oncol. 1997; 28:175–188. [PubMed: 9024511]
13. Clynes D, Higgs D, Gibbons RJ. The chromatin remodeller ATRX: a repeat offender in human disease. Trends in Biochemical Sciences. 2013; 38:461–466. [PubMed: 23916100]
14. Letouzé E, et al. SNP array profiling of childhood adrenocortical tumors reveals distinct pathways of tumorigenesis and highlights candidate driver genes. J Clin Endocrinol Metab. 2012; 97:E1284–E1293. [PubMed: 22539591]
15. Forment JV, Kaidi A, Jackson SP. Chromothripsis and cancer: causes and consequences of chromosome shattering. Nat Rev Cancer. 2012; 12:663–670. [PubMed: 22972457]
16. Nik-Zainal S, et al. Breast Cancer Working Group of the International Cancer Genome Consortium. Mutational processes molding the genomes of 21 breast cancers. Cell. 2012; 149:979–993. [PubMed: 22608084]
17. Oren M. Decision making by p53: life, death and cancer. Cell Death Differ. 2003; 10:431–442. [PubMed: 12719720]
18. Nichols KE, et al. Germ-line p53 mutations predispose to a wide spectrum of early-onset cancers. Cancer Epidemiol Biomarkers Prev. 2001; 10:83–87. [PubMed: 11219776]
19. Ruijs MW, et al. TP53 germline mutation testing in 180 families suspected of Li- Fraumeni syndrome: mutation detection rate and relative frequency of cancers in different familial phenotypes. J Med Genet. 2010; 47:421–428. [PubMed: 20522432]

20. Bischoff FZ, et al. Spontaneous abnormalities in normal fibroblasts from patients with Li-Fraumeni Cancer Syndrome: Aneuploidy and immortalization. Cancer Res. 1990; 50:7979–7984. [PubMed: 2253239]
21. Liu PK, et al. Analysis of genomic instability in Li-Fraumeni fibroblasts with germline p53 mutations. Oncogene. 1996; 12:2267–2278. [PubMed: 8649766]
22. Ehrlich M. DNA methylation in cancer: too much, but also too little. Oncogene. 2002; 35:5400–5413. [PubMed: 12154403]
23. Feinberg AP, Tycko B. The history of cancer epigenetics. Nat Rev Cancer. 2004; 4:143–153. [PubMed: 14732866]
24. Wasserman JD, et al. Prevalence and Functional Consequence of TP53 mutations in Pediatric Adrenocortical Carcinoma: a Children's Oncology Group Study. J Clin Oncol. (manuscript in press).
25. Smith AC, et al. Association of alveolar rhabdomyosarcoma with the Beckwith- Wiedemann syndrome. Pediatr Dev Pathol. 2001; 4:550–558. [PubMed: 11826361]
26. Rainier S, et al. Relaxation of imprinted genes in human cancer. Nature. 1993; 362:747–749. [PubMed: 8385745]
27. Mussa A, et al. Neonatal hepatoblastoma in a newborn with severe phenotype of Beckwith-Wiedemann syndrome. Eur J Pediatr. 2011; 170:1407–1411. [PubMed: 21448630]
28. Gicquel C, et al. Structural and functional abnormalities at 11p15 are associated with the malignant phenotype in sporadic adrenocortical tumors: study on a series of 82 tumors. J Clin Endocrinol Metab. 1997; 82:2559–2565. [PubMed: 9253334]
29. Assie G, et al. Integrated genomic characterization of adrenocortical carcinoma. Nat Genet. 2014; 46:607–612. [PubMed: 24747642]
30. Sun FL, Dean WL, Kelsey G, Allen ND, Reik W. Transactivation of Igf2 in a mouse model of Beckwith-Wiedemann syndrome. Nature. 1997; 389:809–815. [PubMed: 9349812]
31. Heaton JH, et al. Progression to adrenocortical tumorigenesis in mice and humans through insulin-like growth factor 2 and β-catenin. Am J Pathol. 2012; 181:1017–1033. [PubMed: 22800756]
32. Ehrlich PF, et al. Clinicopathologic findings predictive of relapse in children with stage III favorable-histology Wilms tumor. J Clin Oncol. 2013; 31:1196–1201. [PubMed: 23382471]
33. Parham DM. Pathologic classification of rhabdomyosarcomas and correlations with molecular studies. Mod Pathol. 2001; 14:506–514. [PubMed: 11353062]
34. Valentijn LJ, et al. Functional MYCN signature predicts outcome of neuroblastoma irrespective of *MYCN* amplification. Proc Natl Acad Sci USA. 2012; 109:19190–19195. [PubMed: 23091029]
35. El Wakil A, et al. Genetics and genomics of childhood adrenocortical tumors. Mol Cell Endocrinol. 2011; 336:169–173. [PubMed: 21094206]
36. Magro G, et al. Pediatric adrenocortical tumors: morphological diagnostic criteria and immunohistochemical expression of matrix metalloproteinase type 2 and human leucocyte-associated antigen (HLA) class II antigens. Results from the Italian Pediatric Rare Tumor (TREP) Study project. Hum Pathol. 2012; 43:31–39. [PubMed: 21820153]
37. Stratakis CA. Time to individualize treatment for adrenocortical cancer? Nature Reviews Endocrinol. 2014; 10:76–78.
38. Nacheva EP, et al. Human herpesvirus 6 integrates within telomeric regions as evidenced by five different chromosomal Sites. J Med Virol. 2008; 80:1952–1958. [PubMed: 18814270]
39. Morissette G, Flamand L. Herpesviruses and chromosomal integration. J Virol. 2010; 84:12100–12109. [PubMed: 20844040]
40. Huang Y, et al. Human telomeres that carry an integrated copy of human herpesvirus 6 are often short and unstable, facilitating release of the viral genome from the chromosome. Nucleic Acids Res. 2014; 42:315–327. [PubMed: 24057213]
41. Chen X, et al. Targeting oxidative stress in embryonal rhabdomyosarcoma. Cancer Cell. 2013; 24:710–724. [PubMed: 24332040]
42. Zhang J, et al. The genetic basis of early T-cell precursor acute lymphoblastic leukaemia. Nature. 2012; 481:157–163. [PubMed: 22237106]

43. Zhang J, et al. A novel retinoblastoma therapy from genomic and epigenetic analyses. Nature. 2012; 481:329–334. [PubMed: 22237022]
44. Wang J, et al. CREST maps somatic structural variation in cancer genomes with base-pair resolution. Nat Methods. 2011; 8:652–654. [PubMed: 21666668]
45. Li H, Durbin R. Fast and accurate short read alignment with Burrows-Wheeler transform. Bioinformatics. 2009; 25:1754–1760. [PubMed: 19451168]
46. Trapnell C, et al. Transcript assembly and quantification by RNA-Seq reveals unannotated transcripts and isoform switching during cell differentiation. Nat Biotechnol. 2010; 28:511–515. [PubMed: 20436464]
47. Pounds S, et al. A genomic random interval model for statistical analysis of genomic lesion data. Bioinformatics. 2013; 29:2088–2095. [PubMed: 23842812]
48. Parker M, et al. The Pediatric Cancer Genome Project. Assessing telomeric DNA content in pediatric cancers using whole-genome sequencing data. Genome Biol. 2012; 13:R113. [PubMed: 23232254]
49. Leite JL, Stolf HO, Reis NA, Ward LS. Human herpesvirus type 6 and *type 1* infection increases susceptibility to nonmelanoma skin tumors. Cancer Lett. 2005; 224:213–219. [PubMed: 15914272]
50. Arbuckle JH, et al. The latent human herpesvirus-6A genome specifically integrates in telomeres of human chromosomes in vivo and in vitro. Proc Natl Acad Sci USA. 2010; 107:5563–5568. [PubMed: 20212114]

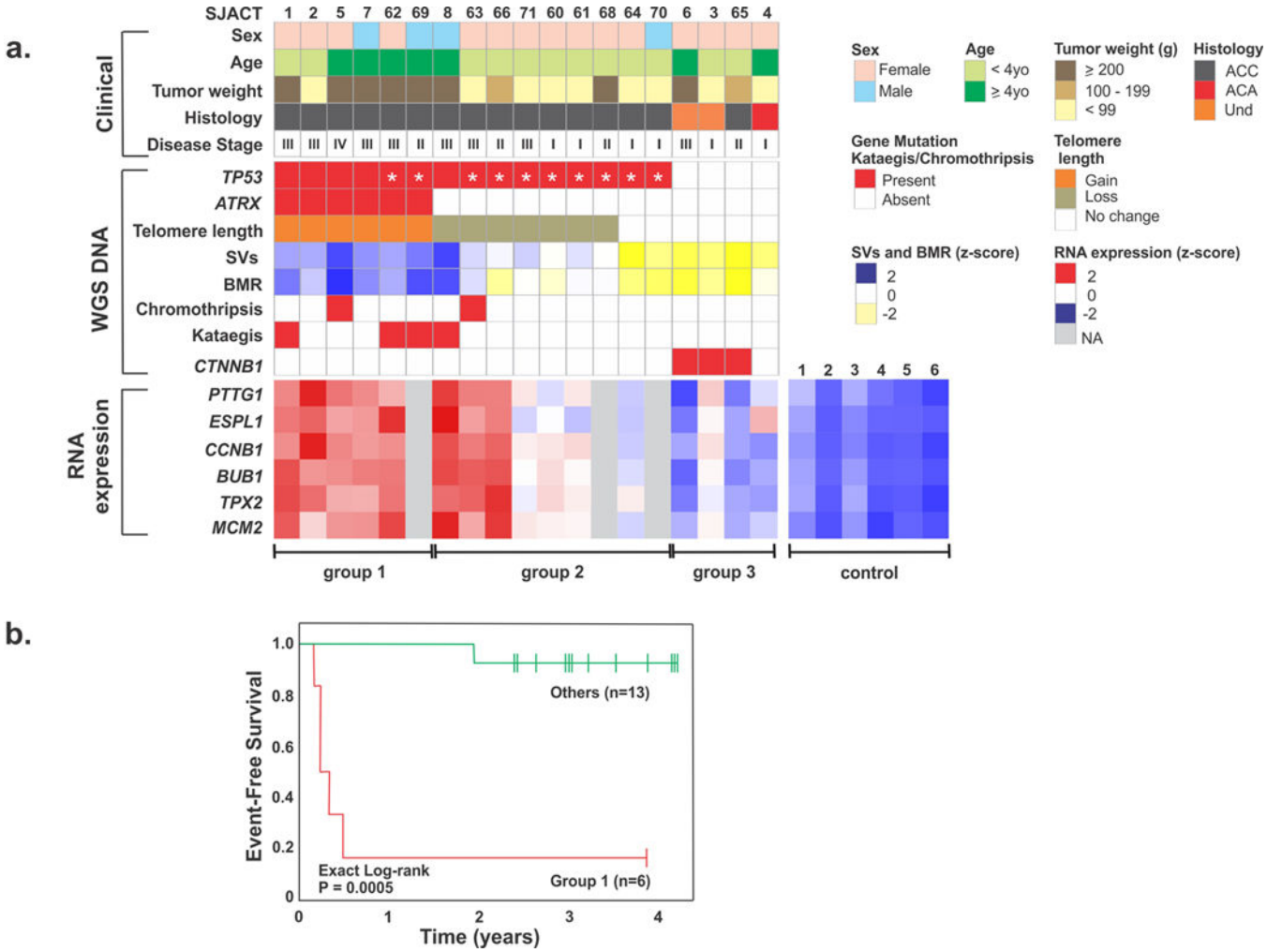

Figure 1.

Association between molecular and clinicopathological features of pediatric adrenocortical tumors. (**a**) Upper panel: clinicopathological features of 19 patients in the WGS cohort. Center panel: genetic alterations, including mutational status of *TP53* (R337H identified by asterisk), *ATRX* and *CTNNB1;* telomere length; number of structural variations (SVs); background mutation rate (BMR); chromothripsis and kataegis. Und: undetermined malignancy. Lower panel: RNA expression of selected genes involved in chromosomal segregation and cell cycle control. Three distinct tumor groups (labeled below) emerged from this analysis. Control: normal adrenocortical tissue. (**b**) Kaplan-Meier probability of event-free survival (exact log-rank test) of pediatric ACT patients in group 1 vs. others.

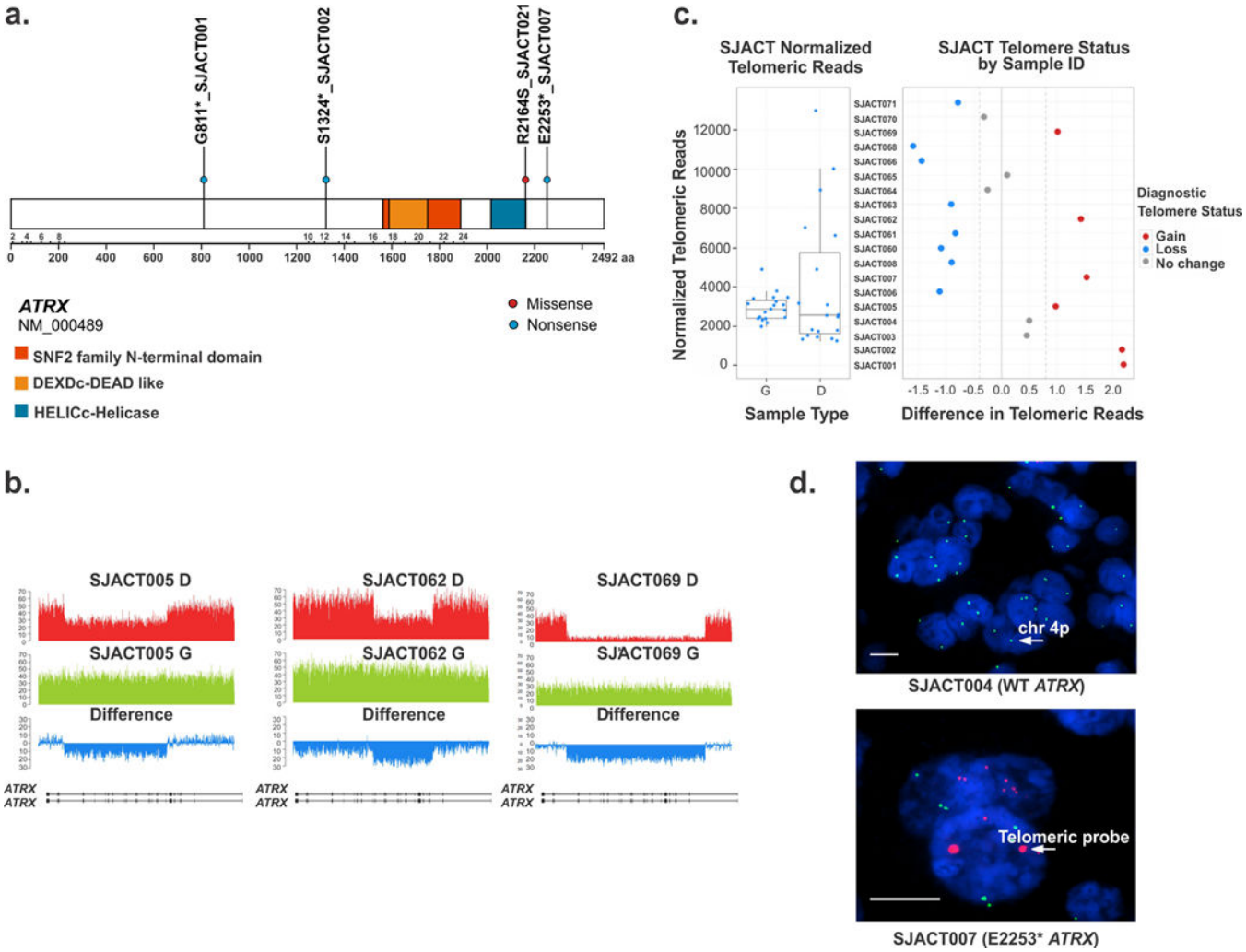

Figure 2.

Somatic *ATRX* mutations and telomere analysis of pediatric adrenocortical tumors. (**a**) Distribution of non-silent single nucleotide variations in *ATRX* (blue dots: nonsense mutations; red dot: missense mutation). (**b**) Wiggle plots showing internal deletion of multiple exons in *ATRX* gene in SJACT005, SJACT062, and SJACT069 (diagnostic tumor [D] and germline [G] samples). (**c**) Relative telomere length determined by WGS in pediatric ACTs vs. matched germline samples. (**d**) Images of tumor samples hybridized with the telomeric FISH (red) and chromosome 4p (green) probes and stained with DAPI to visualize the nucleus (blue). High magnification views show the large, ultrabright signal in *ATRX*-mutant adrenocortical tumor cells (SJACT007). Scale bars, 1 μm.

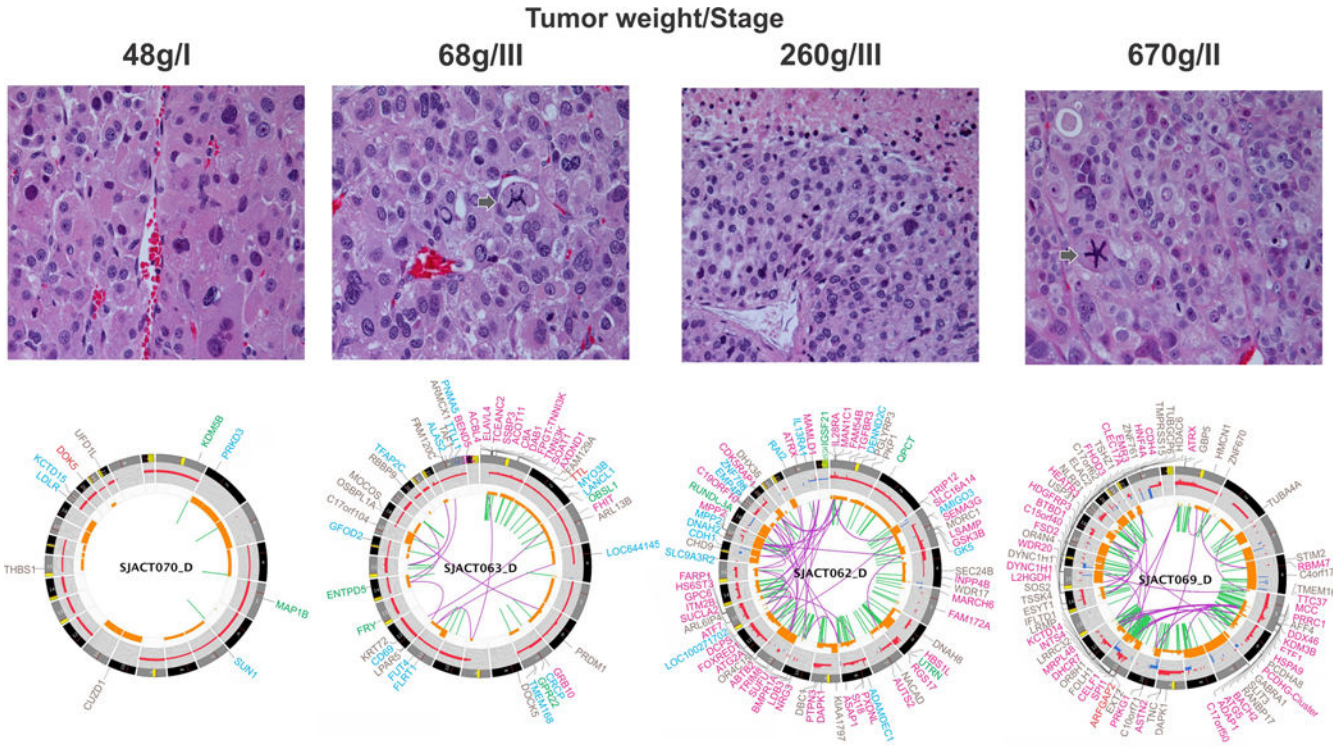

Figure 3.

Histopathological and genomic features of *TP53*-R337H associated ACTs. All tumors had a high mitotic rate (>5 per 50 high-power fields, H&E, 400X). Histology showed a vague nested and trabecular pattern with occasional unpatterned cellular sheets of variable size. Three cases (SJACT063, SJACT062 and SJACT069) had a high nuclear grade and marked cellular pleomorphism. SJACT070 showed occasional enlarged hyperchromatic nuclei with one or more prominent nucleoli. Necrotic cells and atypical mitotic figures (arrow) are identified in SJACT63 and SJACT69. Accumulation of genomic alterations illustrated by the Circos plots (bottom panels) paralleled an increase in tumor weight and correlated with a more aggressive tumor phenotype (Group 1 vs Group 2). Note: labels for gene disrupting SVs (SJACT063 and SJACT062) and non-coding mutations (SJACT069) were removed from the Circos plots.

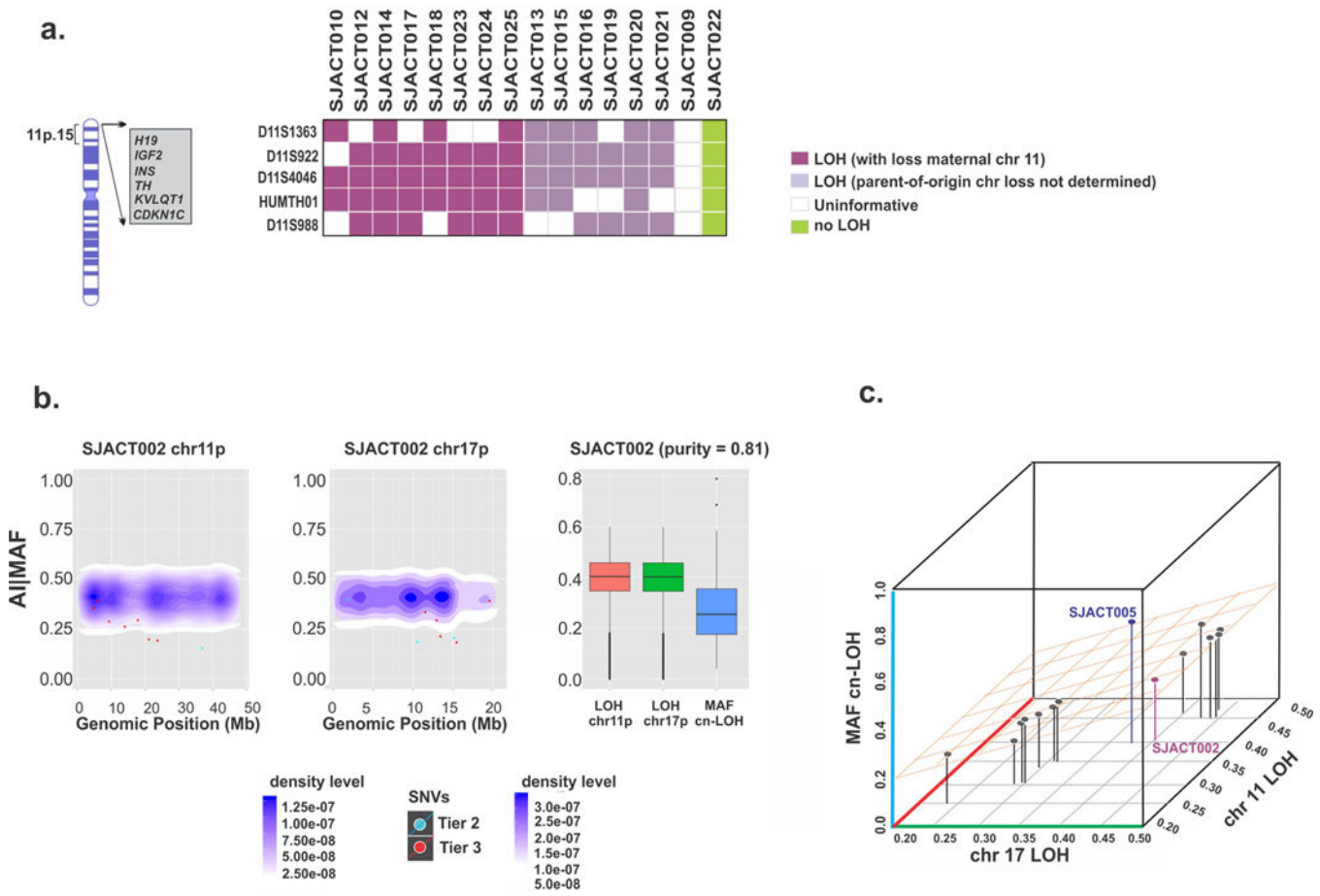

Figure 4.

Characterization and timing of chromosome 11 and 17 LOH in pediatric ACT. (**a**) Microsatellite analysis of chromosome 11p15 in the WES cohort. All cases with available parental DNA demonstrated selective loss of maternal chromosome 11p15 (n=8, purple). (**b**) Temporal order of chromosome 11p and 17p cn-LOH and accumulation of single nucleotide variations (SNVs) in SJACT002. Scatter plots show mutant allele fractions (MAFs) of somatic SNVs and their genomic positions (individual dots) combined with 2-D density plots of allelic imbalance (AI) values of germline heterozygous SNPs in cn-LOH regions of chromosomes 11p (left) and 17p (center). At right, AI values in cn-LOH regions of chromosomes 11p and 17p were compared with the MAF distribution of somatic SNVs in genome-wide cn-LOH regions. (**c**) A 3-D scatter plot summarizes the temporal order of cn-LOH of chromosomes 11p and 17p and somatic SNV accumulation in pediatric ACTs. Shown are median AI values for the chromosome 11p cn-LOH region, median AI values for the chromosome 17p cn-LOH region and median MAF of SNVs in genome-wide cn-LOH regions of 14 cases; SJACT002 and SJACT005 are labeled. See also Supplementary Fig. 7b.

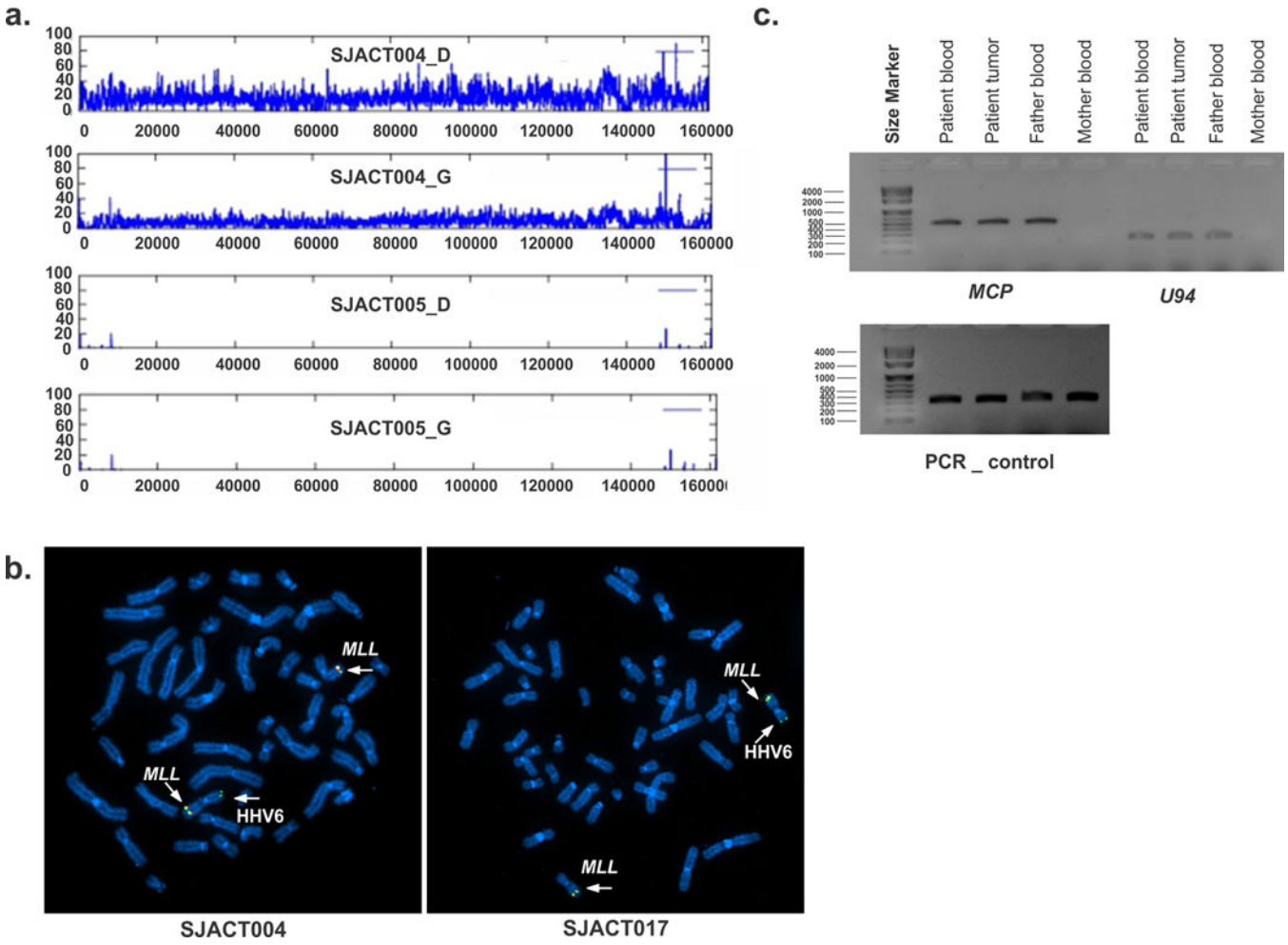

Figure 5.

Chromosomal integration of human herpesvirus 6 in pediatric ACT. (**a**) Coverage plot for cases SJACT004 and SJACT005 showing diagnostic tumor (D) and germline (G) samples reveals integration of the full-length HHV6 genome in SJACT004. The HHV6 genome is duplicated in the tumor sample as a consequence of cn-LOH. (**b**) Fluorescence in situ hybridization (FISH) of metaphase chromosomes from peripheral blood confirmed HHV6 integration at 11p in both cases. The *MLL* probe (chromosome 11q23) was used as control (left, SJACT004; right, SJACT017). (**c**) HHV6 *MCP* (major capsid protein) and *U94* were amplified by PCR from SJACT017 (germline and tumor) and parental DNA demonstrating paternal vertical transmission of integrated HHV6. Exon 6 of the *TP53* gene was amplified as DNA quality control.